TÉCNICO LISBOA

Blinding of a drone with a high-powered laser

Emanuel João Gonçalves Camacho

Report elaborated for the curricular unit

Project in Aerospace Engineering

Advisor(s)/Supervisor(s): Prof. Daniel Silvestre
Prof. Alexandre Bernardino

January 2026

Executive Summary

The wide availability of Unmanned Aerial Vehicles (UAVs) has created new privacy and security challenges, made worse by the spread of low-cost commercial drones. Due to safety concerns, collateral effects, or even high costs per drone intercepted, traditional counter-UAVmethods such as kinetic interception or RF jamming are often unsuitable for urban or law enforcement applications. High-power laser defence systems have recently begun appearing as an alternative, but these tend to be expensive and complex because they rely on kilowatt-class lasers designed to destroy a drone's structure.

This thesis looks at a variant of the above interception strategy: neutralizing a UAVs optical sensors with high-precision, lower power lasers. This method reduces hardware requirements while placing strict demands on the gimbal control, tracking, and targeting subsystems. The research problem is framed around a UAVmoving along a certain trajectory, whose position and velocity are estimated by a visual detection system. These measurements drive a gimbal mounted laser, whose ability to remain aligned with the target determines success.

The main objective of the project is to assess the feasibility of the concept under realistic operating conditions. This requires developing several mathematical models of the gimbal, integrating them with an appropriate control system and sweeping strategy, and evaluating their combined impact on the Time on Target (TOT). Factors outside the project scope like mechanical designs or laser performance are based on industry available data.

Through simulation, the project will generate interception envelopes for different modelling and control choices and evaluate performance across nominal and evasive target scenarios.

Contents

List of Tables

List of Figures

Acronyms

C-UAS Counter-Unmanned Aerial Systems. 3, 23

DOF Degrees of Freedom. 5

EKF Extended Kalman Filter. 3

HEL High Energy Laser. 3

NE Newton-Euler. iii, 2, 12, 14–19, 23

TOT Time on Target. i, 5, 6, 21, 23

UAV Unmanned Aerial Vehicle. i, 1, 3, 5, 21, 23

YOLO You Only Look Once. 3

Chapter 1

Introduction

1.1 Motivation

The proliferation of drone technology throughout the whole wide world has now reached a point where even the most inexperienced user, with basic resources that can be acquired from the internet, may pose a serious risk to the security and or privacy of individuals. For that reason, the suppression of these machines has been a very large priority, especially after the central role they've had in international conflicts such as the Russo-Ukrainian war [2].

Suppressing a drone can be done in a multitude of ways. The main problem with the previous iteration of solutions is their reliance on expensive (in the economic warfare sense) methods which may produce unacceptable collateral for more urban, specifically policing scenarios (such as kinetic and jamming interception-based methods). A more elegant approach is the usage of high-powered lasers that focus the optical unit of the drone itself. This allows the incapacitation of one of the main sensors of the drone, hence nearly completely nullifying the threat while solving the aforementioned issues with the alternatives.

The existence of laser defence systems is however not a new phenomenon. In fact, it is increasingly more widespread, being adopted by many militaries around the world such as the "Iron Beam" developed by Rafael and delivered to the Israeli military [3] on the 28th of December 2025. The way this current iteration of systems works is by compromising the overall structural integrity of the whole drone with kilowatts of power which can be advantageous in certain scenarios, but at the cost of greater complexity and cost for the laser.

In this report an alternative solution is proposed by shifting the focus to (albeit still high-powered) lower-powered lasers that target the optical sensors of the UAVs. In essence, we're trading an increase of the complexity of the tracking and targeting systems for simpler, less powerful lasers that, aside from the cost factors, allow for operations within more restrictive environments.

1.2 Related Work

The increasing relevance of drones in recent years, especially when talking about the defence sector, naturally leads to a lot of research being made around this topic. For that reason, there was enough material to facilitate the researching of related work in an organized, top-down structure, starting with more general papers and then getting specific about certain sub-systems. In general, three main areas of study were identified: the physical modelling of the gimbal, the laser, and the visual tracking system.

A study by E. Kuantama et al. (2024) [4] stood out as one of the few that seriously explored the exact

concept of suppressing drones by targetting their optical sensors with lasers. The main problem with their approach however was the small application scale, especially in terms of range, and so even if the results show some promise for the proof of concept, it remains far from real-world application. With this, it was decided to move further down the so-called top-down structure, looking for subsystem-specific studies that can provide alternative solutions and hopefully improve the results.

1.2.1 Gimbal

Starting with the gimbal, it was clear that the format of the mathematical modelling of the physics was not consensual. In short, the existing models can be divided into three categories : a NE based approach using basic mechanics equations to describe the interactions; the Lagrangian approach, which is based on evaluating the energy of the system; and Kane's method, often preferred for its ability to reduce the number of coordinates while avoiding dealing directly with constraint forces [5]. Although these approaches differ in formulation, most authors arrive at similar simplified representations of the gimbal motion, with the main distinctions lying in how certain assumptions or non-linearities are grouped (more information on this in the following chapter). It is also noteworthy that the models can all be derived from the same referential and quantities that will be defined further down.

Some papers such as [6], based on Lagrange, focused only on this very subject, providing valuable results regarding the accuracy of the method and the simplifications made to the model. Huang Q. et al. mention in [5] how Kane's method is utilized and conclude that it "avoids considering the hinge constraint forces between rigid bodies in the Newton–Euler method and eliminates the need to calculate second-order derivatives in Lagrange". Finally, M. H. Ahmad et al. in [7] present a Newton based modelling alongside a control solution for said model.

Paper	Authors	Model	Key Observations
[6]	Betril Ekstrand	Lagrange	Inertia disturbances can be eliminated by symmetric conditions.
[8]	Y. Bai et al.	Lagrange	Coupling inertia terms, Coriolis and centrifugal forces can be neglected compared with the inertia terms.
[5]	Q. Huang et al.	Kane	Avoids "hinge constraint forces between rigid bodies in the NE method and eliminates the need to calculate second-order derivatives in Lagrange".
[7]	M. H. Ahmad et al.	Newton	Motion about one axis produces reaction torques on the other axis. This cross-coupling becomes stronger at high angular velocities and must be included in accurate models.
[9]	E. Poyrazoğlu	Newton	Mechanical coupling between the inner and outer axes often leads to undesired dynamic interactions which motivates decoupling.
[1]	H. Park et al.	Newton	More controller specific but presents a clearer NE dynamics model definition.

Table 1.1: Literature categorization for gimbal dynamics

1.2.2 Visual Tracking and State Estimation

The visual tracking system will be responsible for the detection and continuous tracking of the drone via a bounding box that delimits the target. Information is extracted in pixels and so it requires post-processing into a usable Cartesian coordinate system which will be explored later on.

Starting with the range detection of UAVs, it was decided to use the ”Known Size Method” also called ”Monocular Scaling”, which relies on the geometric principles of the pinhole camera model. In simpler terms, the size of the detected drone is known to the detection system (presupposes a drone data base existing) and based on what is seen by the optical sensor, range is estimated.

The geometric formulation for this aims to obtain D, defined as the distance from the camera sensor to the drone, inversely proportional in nature to the width of the drone's bounding box in pixels (bigger distance, smaller picture). Given the real-world width of the drone W, the focal length of the camera in pixels f, and the width of the bounding box output by the You Only Look Once (YOLO) detector w_{px}, the distance is calculated in the following manner

$$D = \frac{W f}{w_{px}} \tag{1.1}$$

with f being derived from the camera's horizontal field of view (θ) and the image width in pixels (L):

$$f = \frac{L/2}{\tan(\theta/2)} \tag{1.2}$$

While the YOLO algorithm provides efficient real-time detection, the resulting bounding boxes have what's called localization error. This error manifests itself as pixel jitter, where the bounding box dimensions fluctuate between frames despite the drone remaining at a constant distance. Recent studies by Alshaer et al. [10] and Koksal et al. [11] indicate that these errors are particularly pronounced for small, fast-moving objects like micro-UAVs, where a 1-2 pixel deviation in w_{px} can lead to significant depth estimation errors especially at longer ranges.

Furthermore, the ”tightness” of the bounding box often fails to account for drone orientation (pitch and roll). As noted in the ADG-YOLO framework [12], the projected width of a drone changes with its attitude, leading to an overestimation of distance if the model assumes a static horizontal profile. A very important fact is that the pixel jitter and all aforementioned imperfections with the system must be fed into the signal itself before conversion into Cartesian coordinates in order to maintain the realism of the simulation.

To mitigate the impact of bounding box noise and improve positional stability, an Extended Kalman Filter (EKF) is proposed as a solution. The EKF treats the YOLO output as a noisy measurement and uses a constant velocity motion model to predict the drone's state $x = [x, y, w, h, \dot{x}, \dot{y}]^{\mathsf{T}}$. This smoothing process effectively filters out high-frequency ”jitter” in the centre point and bounding box width, resulting in a more robust distance estimation over time [10].

Another factor that needs to be considered in order to make this system realistic are the errors in tracking which may be divided into two : The losing of the tracking (which will require locking onto the drone once again) and *phantoms* or false positives when the tracking system locks into an undesired object.

1.2.3 Laser

The effectiveness of a High Energy Laser (HEL) system is defined by its ability to deliver energy to the target optical sensor surface. In Counter-Unmanned Aerial Systems (C-UAS) operations, the objective is typically divided between *hard kills* (structural destruction) and *soft kills* (sensor blinding or dazzling).

Modern applications of these systems vary; some of them are higher-power systems such as Raytheon's HELWS $50\,\mathrm{kW}$ system or Rafael's Iron Beam $100\,\mathrm{kW}$ laser, dedicated to large objects such as loitering munitions, rockets, artillery and mortars, as well as drones from categories I, II and III. These systems are utilized to compromise airframes within mere seconds of irradiation time, while smaller-scale sys-

tems with power ranging between $10\,\mathrm{kW}$ to $15\,\mathrm{kW}$ are typically employed against Class I/II drones at ranges of $1\,\mathrm{km}$ to $3\,\mathrm{km}$. Such systems often complement higher-power solutions, as is the case with Rafael's Lite Beam.

Having discussed the current market, it is important to note that the scope of this project targets significantly lower power ratings, potentially even in the hundreds of W range, sufficient to suppress commonly found optical sensors in drone systems such as CMOS and CCDs. This suppression may take the form of either permanent blinding or temporary "dazzling", the latter requiring substantially less energy than structural destruction.

Temporary dazzling is defined as the condition in which the incident irradiance exceeds the sensor's saturation threshold, typically in the $\mathrm{mW\,cm^{-2}}$ range. Once saturated, the sensor requires at least one integration and readout cycle before useful imaging can resume. For modern CMOS sensors operating at video frame rates, recovery typically occurs within a single frame period due to parallel pixel readout, whereas CCD-based systems, which rely on serial charge transfer and longer integration and readout cycles, can exhibit substantially longer recovery times, particularly under high irradiance conditions [13].

Permanent blinding, by contrast, involves irreversible thermal damage to the sensor. Research by Zhilong Jian *et al.* indicates that a localized energy density of approximately $78.9\,\mathrm{mJ\,cm^{-2}}$ delivered within $150\,\mathrm{ns}$ is sufficient to cause permanent damage to individual pixels while preserving the integrity of the metal interconnects between neighboring pixels [14]. The same study reports that increasing the energy density to $2005.4\,\mathrm{mJ\,cm^{-2}}$ results in complete structural failure of the CMOS sensor.

The utilization of lasers is not as straightforward as simply providing sufficient source power to achieve the required irradiance at the target. Atmospheric effects such as diffusion and attenuation introduce significant propagation imperfections, chief among them being:

1. Absorption and Scattering: Commonly modeled using the Beer–Lambert law, $P(z) = P_0 e^{-\gamma z}$. In light fog conditions, the extinction coefficient γ may reach values between $20\,\mathrm{dB\,km^{-1}}$ to $90\,\mathrm{dB\,km^{-1}}$, significantly reducing the effective operational range.

2. Turbulence (Beam Wander): Fluctuations in the atmospheric refractive index, characterized by the structure parameter C_n^2, cause beam jitter and wandering. Near the ground (altitudes below $100\,\mathrm{m}$), typical values of C_n^2 range from $1 \times 10^{-14}\,\mathrm{m^{-2/3}}$ to $1 \times 10^{-13}\,\mathrm{m^{-2/3}}$, which can result in spot displacements of several centimeters over a $1\,\mathrm{km}$ propagation path.

3. Thermal Blooming: High-power beams heat the surrounding air, inducing refractive index gradients that act as a diverging lens and lead to beam defocusing.

4. Focal Length: Laser beams exhibit a conical geometry, initially converging to a minimum cross-sectional area at the focal point. Beyond this point, beam divergence increases, leading to a growing spot size and reduced irradiance.

Finally, one of the most critical challenges in using lasers as a medium of energy transfer is the incidence angle at which the beam strikes the target surface. This angle, denoted here by θ, results in a reduction of the effective transferred power, as observed in [15]. While multiple factors influence this behaviour such as the deformation of the beam cross section from circular to elliptical a first order approximation is provided by Lambert's cosine law. According to this law, the irradiance I is related to the normal-incidence irradiance I_0 by

$$I = I_0 \cos\theta.$$

1.3 Problem Overview

The setup for this research project starts with a UAV flying in a certain pattern. This motion is then tracked by a visual detection system, which will only appear as an uncertainty in the position and velocity vector values of the drone in question. The positional information from the aforementioned system is then fed into a gimbal-laser system with 2 Degrees of Freedom (DOF).

After achieving alignment between the gimbal focal point (where the laser is placed) and the drone, a laser beam is fired which, even in cloudless, rainless weather conditions will be affected by different atmospheric variables. The effects of the laser on the optical sensor will depend upon the amount of power transferred, a function of factors such as the incidence angle, diffusion of the beam and TOT, all of them determining factors for a successful firing event.

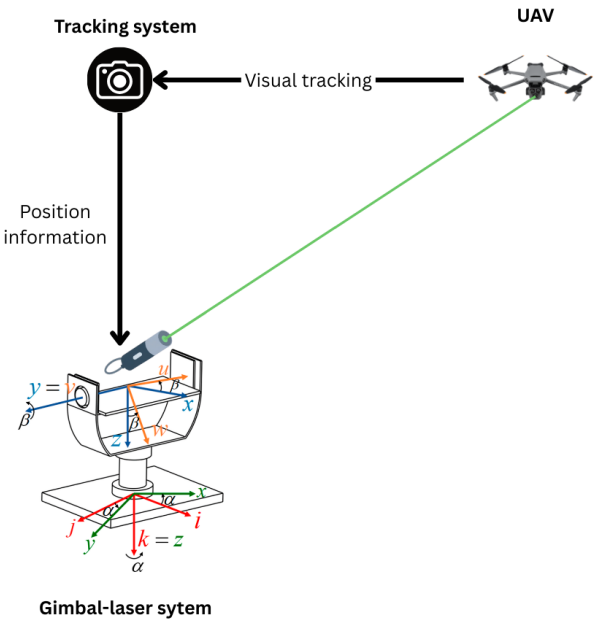

Figure 1.1: Problem setup with gimbal extracted from [1]

1.4 Research Objectives

The overall objective of this research project is to evaluate the feasibility of the previously described laser interception system for a range of realistic operating conditions.

To achieve this, we must first develop a mathematical model that accurately captures the physics of the gimbal. Multiple modelling approaches will be considered, which will interact differently with the control system. Because it is difficult to predict a priori how the various components will respond to the nuances in each model, simulations will be used to identify the most effective approach. Although the visual tracking subsystem is not the primary focus, it remains essential to the overall interception process and its imperfections need to be considered in order to realistically test the concept.

More specifically, the project aims to evaluate different approaches across several stages of the problem. Three alternative physical models of the gimbal will be tested. Combined with the control system

and the sweeping protocol, these will lead to different values of the total TOT. Parameters outside the scope of the research such as the detailed mechanical design of the gimbal, performance characteristics of the laser, and behaviour of the visual tracking system, will be based on representative industry values, some already presented before. The variable factors studied are:

- Physics modelling of the gimbal
- Power of the laser
- Sweeping strategy

By systematically combining these factors, the project will generate a set of interception envelopes corresponding to different modelling and control choices.

1.5 Overview of the Structure

The structure of this project can be divided into 5 main chapters:

- **Chapter** 1: Introduces the topic, summarises the literary research and explains the basic problem setup.
- **Chapter** 2: Provides the theoretical introduction to the gimbal physics modelling and control system.
- **Chapter** 3: Outlines the future work to be done.
- **Chapter** 4: Evaluates the project contribution.

Chapter 2

Theory

2.1 Gimbal definition

The first step in modelling the gimbal is to set up the coordinate framework used throughout this work. The adopted reference configuration is based on the formulation proposed by H. Park et al. [1], chosen for its clarity, simplicity, and close correspondence with the other gimbal models reviewed in the literature section above. A schematic representation of the system is shown in Figure 2.1. The orientation of the gimbal is described using the Euler angles α and β, which naturally leads to a Newton–Euler and Lagrange–Euler formulation.

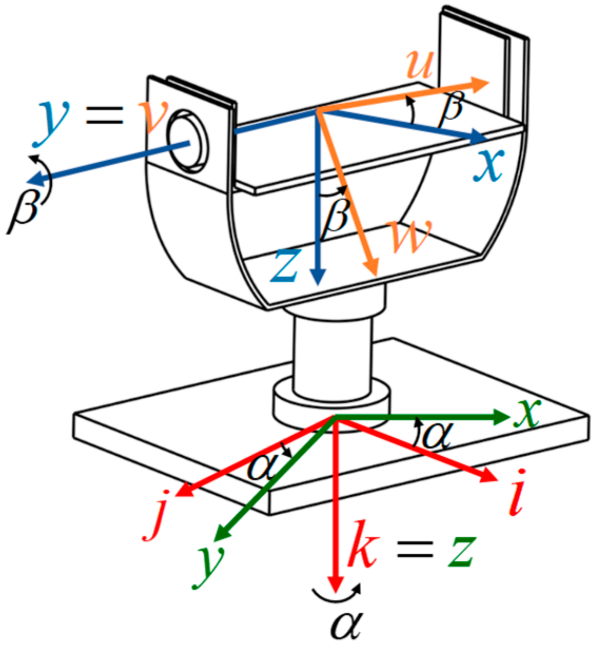

Figure 2.1: Two-degree-of-freedom gimbal configuration and associated reference frames.

A reference frame B is fixed to the stationary base of the gimbal and defined by the orthonormal axes $(\vec{i}, \vec{j}, \vec{k})$. The yaw frame K, described by the axes $(\vec{x}, \vec{y}, \vec{z})$, is attached to the yaw gimbal and results from a rotation of angle α about the $\vec{k}$ axis of frame B. Finally, the pitch frame A, defined by the axes $(\vec{u}, \vec{v}, \vec{w})$, is fixed to the pitch gimbal and is obtained by a rotation of angle β about the $\vec{y}$ axis of frame K. The laser is fixed to this last frame, with its pointing direction aligned with the $\vec{u}$ axis.

The kinematic relationship between the reference frames is described through the rotation matrices

$$L_{KB} = \begin{bmatrix} \cos\alpha & \sin\alpha & 0 \\ -\sin\alpha & \cos\alpha & 0 \\ 0 & 0 & 1 \end{bmatrix}, \qquad L_{AK} = \begin{bmatrix} \cos\beta & 0 & -\sin\beta \\ 0 & 1 & 0 \\ \sin\beta & 0 & \cos\beta \end{bmatrix}. \tag{2.1}$$

Matrix L_{KB} transforms vectors expressed in the base frame B into the yaw frame K, while L_{AK} performs the transformation from the yaw frame to the pitch frame. For instance, a vector $\vec{v}_B$ expressed in frame B can be written in frame K as $\vec{v}_K = L_{KB}\vec{v}_B$.

Angular velocities are now defined for each reference frame as

$$\vec{\omega}_B = \begin{bmatrix} \omega_i \\ \omega_j \\ \omega_k \end{bmatrix}, \qquad \vec{\omega}_K = \begin{bmatrix} \omega_x \\ \omega_y \\ \omega_z \end{bmatrix}, \qquad \vec{\omega}_A = \begin{bmatrix} \omega_u \\ \omega_v \\ \omega_w \end{bmatrix}. \tag{2.2}$$

Since the base frame is assumed to be fixed in inertial space, its angular velocity is identically zero, that is $\vec{\omega}_B = \vec{0}$. The angular velocity of the yaw frame K is obtained by expressing the contribution of the base frame (which is 0 as previously stated) and then adding the rotation rate $\dot{\alpha}$ about the $\vec{k}$ axis, relative to the base frame. This yields

$$\vec{\omega}_K = L_{KB}\vec{\omega}_B + \begin{bmatrix} 0 \\ 0 \\ \dot{\alpha} \end{bmatrix} = \begin{bmatrix} 0 \\ 0 \\ \dot{\alpha} \end{bmatrix}, \tag{2.3}$$

and the same procedure can be used to calculate the angular velocity of the pitch frame A. It is obtained by transforming $\vec{\omega}_K$ into frame A and adding the relative rotation rate $\dot{\beta}$ about the $\vec{y}$ axis of frame K, resulting in

$$\vec{\omega}_A = L_{AK}\vec{\omega}_K + \begin{bmatrix} 0 \\ \dot{\beta} \\ 0 \end{bmatrix} = \begin{bmatrix} \dot{\alpha}\sin\beta \\ \dot{\beta} \\ \dot{\alpha}\cos\beta \end{bmatrix}. \tag{2.4}$$

Another fundamental quantity required by all subsequent dynamic models is the inertia of the yaw and pitch gimbals. These are represented in tensor form by the inertia matrices

$$J_K = \begin{bmatrix} Y_{xx} & Y_{xy} & Y_{xz} \\ Y_{xy} & Y_{yy} & Y_{yz} \\ Y_{xz} & Y_{yz} & Y_{zz} \end{bmatrix}, \qquad J_A = \begin{bmatrix} P_{uu} & P_{uv} & P_{uw} \\ P_{uv} & P_{vv} & P_{vw} \\ P_{uw} & P_{vw} & P_{ww} \end{bmatrix}. \tag{2.5}$$

This concludes the kinematic foundation of the gimbal model and provides the necessary definitions for the development of the different dynamic modelling approaches considered in the following sections.

2.2 Newton-Euler

The derivation of this model starts from the second law of Newton $\vec{F} = m \cdot \vec{a}$ which can be rewritten in its rotational form by considering a torque T applied on a rigid body's centre of mass yielding

$$T = J \cdot \frac{d}{dt}\vec{\omega} + \vec{\omega} \times J \cdot \vec{\omega}. \tag{2.6}$$

Noting that $J \cdot \vec{\omega}$ corresponds to the angular momentum $\vec{H}$ and $\frac{d}{dt}\vec{\omega} = \dot{\vec{\omega}}$ (but in vector form) the angular acceleration. Equation (2.6) can also be applied only to pitch gimbal's v axis, which is very useful as its the axis around which pitch motion is performed, thus producing

$$T_v = \left(J_A \dot{\vec{\omega}}_A\right)_v + \left(\vec{\omega}_A \times J_A \vec{\omega}_A\right)_v \tag{2.7}$$

with $\frac{d}{dt}\vec{\omega_A}$ being obtained by performing the derivative of (2.4) with respect to time :

$$\frac{d}{dt}\vec{\omega}_A = \begin{bmatrix} \ddot{\alpha}\sin\beta + \dot{\alpha}\dot{\beta}\cos\beta \\ \ddot{\beta} \\ \ddot{\alpha}\cos\beta - \dot{\alpha}\dot{\beta}\sin\beta \end{bmatrix} = \dot{\vec{\omega}}_A \tag{2.8}$$

Using the pitch inertia tensor presented in (2.5) we are now able to take equation (2.7) and compute each term, starting with the v (or pitch) component of the acceleration term,

$$\begin{aligned} \left(J_A \dot{\vec{\omega}}_A\right)_v &= P_{uv}\,\dot{\omega}_u + P_{vv}\,\dot{\omega}_v + P_{vw}\,\dot{\omega}_w = \\ &= P_{uv}\big(\ddot{\alpha}\sin\beta + \dot{\alpha}\dot{\beta}\cos\beta\big) + P_{vv}\,\ddot{\beta} + P_{vw}\big(\ddot{\alpha}\cos\beta - \dot{\alpha}\dot{\beta}\sin\beta\big), \end{aligned} \tag{2.9}$$

and very similarly also the angular momentum components of $H_A = J_A\omega_A$,

$$\begin{aligned} H_u &= P_{uu}\,\omega_u + P_{uv}\,\omega_v + P_{uw}\,\omega_w = P_{uu}\dot{\alpha}\sin\beta + P_{uv}\dot{\beta} + P_{uw}\dot{\alpha}\cos\beta \\ H_v &= P_{uv}\,\omega_u + P_{vv}\,\omega_v + P_{vw}\,\omega_w = P_{uv}\dot{\alpha}\sin\beta + P_{vv}\dot{\beta} + P_{vw}\dot{\alpha}\cos\beta \\ H_w &= P_{uw}\,\omega_u + P_{vw}\,\omega_v + P_{ww}\,\omega_w = P_{uw}\dot{\alpha}\sin\beta + P_{vw}\dot{\beta} + P_{ww}\dot{\alpha}\cos\beta. \end{aligned} \tag{2.10}$$

The gyroscopic term in (2.7) : $\left(\vec{\omega}_A \times \vec{H}\right)_v = \omega_w H_u - \omega_u H_w$ is then given by :

$$\left(\vec{\omega}_A \times \vec{H}\right)_v = \dot{\alpha}\dot{\beta}\left(P_{uv}\cos\beta - P_{vw}\sin\beta\right) + \dot{\alpha}^2\Big(\left(P_{uu} - P_{ww}\right)\sin\beta\cos\beta + P_{uw}\cos 2\beta\Big) \tag{2.11}$$

Control-Oriented Decomposition of the Pitch Equation

Having fully derived all terms of equation (2.6), we now need to reframe it into a model suitable for control design. This is done by decomposing the net torque (v) component T_v with the primary objective of isolating the desired acceleration term ($\ddot{\beta}$). All remaining terms are then grouped into the control input (T_E, representing the motor torque) and disturbance torques (T_{DE1}, $T_{DE2} \in \mathbb{R}$).

The rearrangement follows three key steps:

1. Defining the Control Input (T_E): The net torque T_v is replaced by the actuator torque T_E, representing the torque applied by the motor about the v-axis to drive the pitch motion.

2. Isolating the Target Acceleration Term ($\ddot{\beta}$): The term $\ddot{\beta}$ (along with its inertia coefficient) is isolated, as it represents the torque required for pure pitch acceleration, i.e., the inertia that the actuator must overcome.

3. Grouping Disturbance Terms (T_{DE1} and T_{DE2}): All remaining terms are grouped as disturbance torques. These represent torques generated by internal dynamics (inertial and velocity coupling effects) that must be compensated by the actuator torque T_E.

Both T_{DE1} and T_{DE2} are defined such that the final equation expresses the dynamics in the following control-oriented form: required inertial torque equals actuator input plus dynamic disturbances. Combining (2.9) and (2.11), and denoting the actuator torque about the pitch axis by T_E, the pitch-axis scalar equation is obtained,

$$P_{vv}\,\ddot{\beta} \;=\; T_E \;-\; T_{DE1} \;-\; T_{DE2}, \tag{2.12}$$

the disturbance terms being grouped according to their physical origin, following the cross-coupling disturbance interpretation adopted in the literature.

T_{DE1} represents the inertial coupling due to yaw-axis motion. This term collects the disturbance torques generated by yaw-axis angular acceleration and associated transport effects, which are coupled into the pitch axis through the off-diagonal inertia elements (P_{uv} and P_{vw}). These disturbances arise from inertial reactions caused by asymmetric mass distribution during yaw motion.

$$T_{DE1} = P_{uv}\big(\ddot{\alpha}\sin\beta + \dot{\alpha}\dot{\beta}\cos\beta\big) + P_{vw}\big(\ddot{\alpha}\cos\beta - \dot{\alpha}\dot{\beta}\sin\beta\big) \tag{2.13}$$

T_{DE2} represents gyroscopic and centrifugal cross-coupling disturbances. This term groups the remaining quadratic velocity effects originating from the gyroscopic torque $\vec{\omega}_A \times J_A\vec{\omega}_A$. These disturbances are generated by the simultaneous rotation about the yaw and pitch axes and represent non-linear cross-coupling effects that must be compensated by the actuator.

$$T_{DE2} = \dot{\alpha}\dot{\beta}\left(P_{uv}\cos\beta - P_{vw}\sin\beta\right) + \dot{\alpha}^2\Big(\left(P_{uu} - P_{ww}\right)\sin\beta\cos\beta + P_{uw}\cos 2\beta\Big) \tag{2.14}$$

A noteworthy fact of the derivation is that if the tensor J_A is diagonal (in other words the gimbal has perfect symmetry about its principal axes), i.e., $P_{uv} = P_{uw} = P_{vw} = 0$, then $T_{DE1} \equiv 0$ thus simplifying the model.

Control-Oriented Decomposition of the Yaw Equation

Unlike the pitch dynamics, which involve only the pitch gimbal, the yaw actuator must accelerate the entire yaw–pitch assembly. Consequently, the yaw-axis dynamics must be formulated using the total inertia of both gimbals expressed in the yaw frame K.

Applying the Newton–Euler rotational equation to the complete yaw–pitch assembly and extracting the component about the z axis of frame K yields

$$T_z = \left(J_{AZ}\,\dot{\vec{\omega}}_{AZ}\right)_z + \left(\vec{\omega}_{AZ} \times J_{AZ}\,\vec{\omega}_{AZ}\right)_z, \tag{2.15}$$

where $J_{AZ} \in \mathbb{R}^{3\times3}$ denotes the inertia tensor of the complete yaw–pitch assembly expressed in frame K, and $\vec{\omega}_{AZ}$ is its absolute angular velocity.

The inertia tensor J_{AZ} is obtained by summing the yaw gimbal inertia, already expressed in frame K, and the pitch gimbal inertia rotated from frame A into frame K using the rotational matrix defined in (2.1),

$$J_{AZ} = J_K + L_{KA}\,J_A\,L_{KA}^{\mathsf{T}},$$

with $L_{KA} = L_{AK}^{\mathsf{T}}$.

The absolute angular velocity of the yaw–pitch assembly is given by the combined yaw and pitch

rotations expressed in frame K as

$$\vec{\omega}_{AZ} = \begin{bmatrix} 0 \\ \dot{\beta} \\ \dot{\alpha} \end{bmatrix}, \qquad \dot{\vec{\omega}}_{AZ} = \begin{bmatrix} 0 \\ \ddot{\beta} \\ \ddot{\alpha} \end{bmatrix}. \tag{2.16}$$

This angular velocity differs from $\vec{\omega}_K$ defined in (2.3), as it represents the absolute angular velocity of the full yaw–pitch assembly rather than that of the yaw frame alone. We can then expand the z component of the inertial acceleration term in (2.15) as

$$\left(J_{AZ}\,\dot{\vec{\omega}}_{AZ}\right)_z = J_Z\,\ddot{\alpha} + (J_{AZ})_{zy}\,\ddot{\beta}, \tag{2.17}$$

where $J_Z \equiv (J_{AZ})_{zz}$ represents the effective (or z component) yaw-axis inertia of the yaw–pitch assembly. The gyroscopic term's expression can also be derived yielding

$$\left(\vec{\omega}_{AZ} \times J_{AZ}\,\vec{\omega}_{AZ}\right)_z = -\,\dot{\beta}\,H_x, \tag{2.18}$$

with $\vec{H} = J_{AZ}\vec{\omega}_{AZ}$ denoting the angular momentum of the yaw-pitch assembly. Isolating the yaw angular acceleration, just as it was done in the pitch section, yields the control-oriented yaw dynamic equation,

$$J_Z\,\ddot{\alpha} = T_A + T_{DZ}, \tag{2.19}$$

where T_A is the actuator torque applied about the yaw axis. The total disturbance torque $T_{DZ} \in \mathbb{R}$ is given by

$$T_{DZ} = -\Big((J_{AZ})_{zy}\,\ddot{\beta} + \dot{\beta}\,H_x\Big). \tag{2.20}$$

Following the same structure adopted for the pitch axis, the disturbance torque is decomposed into three distinct terms as

$$T_{DZ} = -\big(T_{DA1} + T_{DA2} + T_{DA3}\big), \tag{2.21}$$

with the term T_{DA1} representing cross-axis inertial acceleration coupling due to the off-diagonal elements of the inertia tensor and being given by

$$T_{DA1} = (J_{AZ})_{zy}\,\ddot{\beta}. \tag{2.22}$$

The term T_{DA2} collects gyroscopic and centrifugal coupling effects and is defined as

$$T_{DA2} = \dot{\beta}\,H_x. \tag{2.23}$$

Since the effective yaw inertia J_Z depends on the pitch angle β, its time variation introduces an additional disturbance torque,

$$T_{DA3} = \dot{J}_Z\,\dot{\alpha}, \qquad \dot{J}_Z = \frac{\mathrm{d}J_Z}{\mathrm{d}\beta}\,\dot{\beta}. \tag{2.24}$$

It should be noted that the disturbance decomposition in (2.21) is expressed exclusively in terms of the angular velocity of the yaw–pitch assembly, $\vec{\omega}_{AZ}$, whose components are given in (2.16).

As a final note, T_{DA1}, T_{DA2} and T_{DA3} represent inertial, gyroscopic, and structure dependent coupling effects that can be understood as torques that must compensated by the yaw actuator when performing the desired motion.

2.2.1 Final non-linear Dynamic Model

After the intensive deduction presented before, it is prudent to present, in short, the final non-linear dynamic model of the two-degree-of-freedom gimbal system. The model is expressed in terms of the yaw angle α, the pitch angle β, and their respective time derivatives, with the reasoning being that these variables are what's affected by the control mechanisms of the gimbal (the pitch and yaw motors). In summary, the expression explicitly captures inertial, gyroscopic, and structure dependent coupling effects between the two axes.

Pitch-Axis Dynamic Equation

The pitch-axis dynamics, obtained by applying the NE rotational equation to the pitch gimbal and extracting the component about the v axis of frame A, can be written in the control-oriented form

$$P_{vv}\,\ddot{\beta} = T_E - T_{DE1} - T_{DE2} \tag{2.25}$$

where T_E denotes the actuator torque applied about the pitch axis. The disturbance torques are given by

$$\begin{aligned} T_{DE1} &= P_{uv}\big(\ddot{\alpha}\sin\beta + \dot{\alpha}\dot{\beta}\cos\beta\big) + P_{vw}\big(\ddot{\alpha}\cos\beta - \dot{\alpha}\dot{\beta}\sin\beta\big) \\ T_{DE2} &= \dot{\alpha}\dot{\beta}\left(P_{uv}\cos\beta - P_{vw}\sin\beta\right) + \dot{\alpha}^2\Big(\left(P_{uu} - P_{ww}\right)\sin\beta\cos\beta + P_{uw}\cos 2\beta\Big) \end{aligned} \tag{2.26}$$

The term T_{DE1} represents inertial coupling effects induced by yaw-axis angular acceleration and mixed transport terms, while T_{DE2} collects the quadratic velocity-dependent contributions arising from gyroscopic and centrifugal effects.

Yaw-Axis Dynamic Equation

The yaw-axis dynamics are obtained by applying the NE rotational equation to the complete yaw-pitch assembly and extracting the component about the z axis of the yaw frame K. The resulting scalar equation can be written as

$$J_Z(\beta)\,\ddot{\alpha} = T_A - T_{DA1} - T_{DA2} - T_{DA3} \tag{2.27}$$

where T_A denotes the actuator torque applied about the yaw axis and $J_Z(\beta)$ is the effective yaw-axis inertia. The disturbance torques are defined as

$$\begin{aligned} T_{DA1} &= (J_{AZ})_{zy}\,\ddot{\beta} \\ T_{DA2} &= \dot{\beta}\,H_x \\ T_{DA3} &= \dot{J}_Z(\beta)\,\dot{\alpha} \end{aligned} \tag{2.28}$$

with $\vec{H} = J_{AZ}\vec{\omega}_{AZ}$ denoting the angular momentum of the yaw-pitch assembly and

$$\vec{\omega}_{AZ} = \begin{bmatrix} 0 \\ \dot{\beta} \\ \dot{\alpha} \end{bmatrix}$$

Effective Yaw-Axis Inertia

The effective yaw-axis inertia is obtained by projecting the pitch gimbal inertia onto the yaw axis and adding the yaw gimbal contribution. Using the rotation matrix L_{AK}, the yaw-axis inertia is given explicitly

by

$$J_Z(\beta) = Y_{zz} + P_{uu}\sin^2\beta + 2P_{uw}\sin\beta\cos\beta + P_{ww}\cos^2\beta \tag{2.29}$$

The final model consists of two coupled, non-linear second-order differential equations describing the yaw and pitch dynamics of the gimbal system. The coupling between axes is a consequence of the existence of non-diagonal inertia terms, gyroscopic interactions, and structure based inertia effects. The explicit dependence of the yaw-axis inertia on the pitch angle further highlights the intrinsically non-linear nature of the system. These equations constitute the foundation for the control design, analysis, and simulation approaches developed in the subsequent chapter.

2.3 Lagrange-Euler

An alternative approach to deriving the gimbal dynamics is the Lagrange-Euler formulation, which is based on the energy balance of the system. By using kinetic energy expressions, this method naturally leads to compact, control-oriented equations equivalent to the NE results but this needs to be proven first.

2.3.1 Generalized Coordinates

The generalized coordinates are chosen as the gimbal angles, which is a natural choice given the control objective :

$$\vec{q} = \begin{bmatrix} \alpha \\ \beta \end{bmatrix}, \qquad \dot{\vec{q}} = \begin{bmatrix} \dot{\alpha} \\ \dot{\beta} \end{bmatrix}, \tag{2.30}$$

where α is the yaw angle about the z axis of frame K, and β is the pitch angle about the v axis of frame A. The corresponding generalized torques are

$$\vec{\mathcal{L}} = \begin{bmatrix} T_A \\ T_E \end{bmatrix}, \tag{2.31}$$

with T_A the yaw actuator torque and T_E the pitch actuator torque. It is also useful to remember the angular velocities of the pitch and yaw gimbals defined in (2.4), given by

$$\vec{\omega}_A = \begin{bmatrix} \dot{\alpha}\sin\beta \\ \dot{\beta} \\ \dot{\alpha}\cos\beta \end{bmatrix}, \quad \vec{\omega}_K = \begin{bmatrix} 0 \\ 0 \\ \dot{\alpha} \end{bmatrix}$$

and the also recall the pitch gimbal inertia tensor in frame A

$$J_A = \begin{bmatrix} P_{uu} & P_{uv} & P_{uw} \\ P_{uv} & P_{vv} & P_{vw} \\ P_{uw} & P_{vw} & P_{ww} \end{bmatrix}.$$

We may now write the expression for the kinetic energy of the pitch gimbal as a variation of the well known equation $E_{kinetic} = \frac{1}{2} \cdot m \cdot v^2$, but applied to a rotational frame (using an inertia tensor) :

$$\mathcal{L}_A = \frac{1}{2}\vec{\omega}_A^T J_A \vec{\omega}_A, \tag{2.32}$$

which expands to

$$\begin{aligned} \mathcal{L}_A = \frac{1}{2}P_{vv}\dot{\beta}^2 + \frac{1}{2}\dot{\alpha}^2\Big(P_{uu}\sin^2\beta + 2P_{uw}\sin\beta\cos\beta + P_{ww}\cos^2\beta\Big) \\ + \dot{\alpha}\dot{\beta}\big(P_{uv}\sin\beta + P_{vw}\cos\beta\big). \end{aligned} \tag{2.33}$$

Assuming a scalar yaw-axis inertia Y_{zz}, the yaw gimbal kinetic energy is

$$\mathcal{L}_K = \frac{1}{2}Y_{zz}\dot{\alpha}^2. \tag{2.34}$$

and so the total kinetic energy given by :

$$\mathcal{L} = \mathcal{L}_A + \mathcal{L}_K.$$

2.3.2 Lagrange Equations

Lagrange's equations for each generalized coordinate q_i are simply a rewritten form of energy balance :

$$\frac{d}{dt}\left(\frac{\partial \mathcal{L}}{\partial \dot{q}_i}\right) - \frac{\partial \mathcal{L}}{\partial q_i} = \mathcal{L}_i. \tag{2.35}$$

With the left side of the equation representing the inertial reaction to the torque on the right hand side.

Starting with the pitch equation, the defining angle β is used as the generalized coordinate angle, producing

$$\frac{\partial \mathcal{L}}{\partial \dot{\beta}} = P_{vv}\dot{\beta} + \dot{\alpha}(P_{uv}\sin\beta + P_{vw}\cos\beta),$$

$$\frac{d}{dt}\frac{\partial \mathcal{L}}{\partial \dot{\beta}} = P_{vv}\ddot{\beta} + P_{uv}(\ddot{\alpha}\sin\beta + \dot{\alpha}\dot{\beta}\cos\beta) + P_{vw}(\ddot{\alpha}\cos\beta - \dot{\alpha}\dot{\beta}\sin\beta),$$

$$\frac{\partial \mathcal{L}}{\partial \beta} = \dot{\alpha}\dot{\beta}(P_{uv}\cos\beta - P_{vw}\sin\beta) + \dot{\alpha}^2((P_{uu} - P_{ww})\sin\beta\cos\beta + P_{uw}\cos 2\beta).$$

Substituting into Lagrange's equation gives the control-oriented pitch equation

$$P_{vv}\,\ddot{\beta} = T_E - T_{DE1} - T_{DE2} \tag{2.36}$$

with disturbances

$$T_{DE1} = P_{uv}(\ddot{\alpha}\sin\beta + \dot{\alpha}\dot{\beta}\cos\beta) + P_{vw}(\ddot{\alpha}\cos\beta - \dot{\alpha}\dot{\beta}\sin\beta),$$
$$T_{DE2} = \dot{\alpha}\dot{\beta}(P_{uv}\cos\beta - P_{vw}\sin\beta) + \dot{\alpha}^2((P_{uu} - P_{ww})\sin\beta\cos\beta + P_{uw}\cos 2\beta),$$

exactly matching the NE result. In order to finalize the modelling all that is missing is the yaw axis whose generalized coordinate is the angle α. Using the same method as before to obtain

$$\frac{\partial \mathcal{L}}{\partial \dot{\alpha}}, \quad \frac{d}{dt}\frac{\partial \mathcal{L}}{\partial \dot{\alpha}}, \quad \frac{\partial \mathcal{L}}{\partial \alpha}$$

which yields (deduction omitted as it follows the exact same format) :

$$J_Z(\beta)\,\ddot{\alpha} = T_A - T_{DA1} - T_{DA2} - T_{DA3} \tag{2.37}$$

with

$$J_Z(\beta) = Y_{zz} + P_{uu}\sin^2\beta + 2P_{uw}\sin\beta\cos\beta + P_{ww}\cos^2\beta,$$

and disturbance torques T_{DA1}, T_{DA2}, T_{DA3} as defined in the NE formulation.

2.3.3 Remarks on Equivalence

The Lagrange formulation reproduces the exact same pitch and yaw dynamics as the NE approach. The disturbances T_{DE1}, T_{DE2} (pitch) and $T_{DA1}, T_{DA2}, T_{DA3}$ (yaw) naturally emerge from the energy expressions and represent the same inertial and gyroscopic couplings. The zz entry of the yaw total inertia matrix $(J_{AZ})_{zz} \equiv J_Z(\beta)$ obtained via energy methods matches exactly the NE case. This confirms the equivalence of the gimbal model and validates the control-oriented decomposition adopted for controller design.

2.4 Kane's Method

Kane's method provides a velocity-based formulation of multi-body dynamics using generalized speeds rather than generalized coordinates. When applied consistently, it yields equations of motion that are fully equivalent to those obtained using NE and Lagrange's formulations, while offering additional flexibility in the grouping of dynamic coupling terms.

Using the same gimbal geometry, reference frames, inertia definitions, and kinematic assumptions as in the previous sections, Kane's equations are now derived for the yaw-pitch gimbal assembly.

2.4.1 Generalized Coordinates and Speeds

The generalized coordinates remain

$$q = \begin{bmatrix} \alpha \\ \beta \end{bmatrix},$$

while the generalized speeds are chosen to align directly with the actuated degrees of freedom:

$$u_1 = \dot{\alpha}, \qquad u_2 = \dot{\beta}. \tag{2.38}$$

This choice simplifies the interpretation of the resulting equations, as each generalized speed corresponds directly to a physical actuator. Some assumptions must also be made, namely that : both gimbals are rigid and gravity-balanced; The same reference frames and axis definitions as in the NE and Lagrange formulations are used. Off-diagonal inertia terms such as P_{uv}, P_{vw}, and P_{uw} are retained and finally that the base, like before, is fixed $\vec{\omega}_B = 0$. The angular velocity of the pitch gimbal expressed in frame A is then

$$\vec{\omega}_A = \begin{bmatrix} u_1 \sin\beta \\ u_2 \\ u_1 \cos\beta \end{bmatrix}, \tag{2.39}$$

while the yaw gimbal angular velocity expressed in frame K is

$$\vec{\omega}_K = \begin{bmatrix} 0 \\ 0 \\ u_1 \end{bmatrix}. \tag{2.40}$$

The partial angular velocities associated with each generalized speed are

$$\frac{\partial \vec{\omega}_A}{\partial u_1} = \begin{bmatrix} \sin\beta \\ 0 \\ \cos\beta \end{bmatrix}, \qquad \frac{\partial \vec{\omega}_A}{\partial u_2} = \begin{bmatrix} 0 \\ 1 \\ 0 \end{bmatrix}.$$

Another important quantity to remember is the angular momentum of the pitch gimbal expressed in frame A

$$H_A = J_A \vec{\omega}_A, \tag{2.41}$$

with components

$$H_A = \begin{bmatrix} P_{uu}\omega_u + P_{uv}\omega_v + P_{uw}\omega_w \\ P_{uv}\omega_u + P_{vv}\omega_v + P_{vw}\omega_w \\ P_{uw}\omega_u + P_{vw}\omega_v + P_{ww}\omega_w \end{bmatrix}.$$

2.4.2 Kane's Equations

For each generalized speed u_i, Kane's equation for rotational motion can be written as

$$\frac{d}{dt}\left(\frac{\partial H_A}{\partial u_i}\right) + \vec{\omega}_A \times \frac{\partial H_A}{\partial u_i} = F_i, \tag{2.42}$$

where F_i is the generalized active torque associated with u_i. Starting with the pitch axis, (2.42) is expressed with respect to the generalized speed u_2 (pitch motion), expanding it yields

$$\begin{aligned} &P_{vv}\dot{u}_2 + (P_{uv}\sin\beta + P_{vw}\cos\beta)\dot{u}_1 \\ &\quad + u_1u_2(P_{uv}\cos\beta - P_{vw}\sin\beta) \\ &\quad + u_1^2\Big((P_{uu} - P_{ww})\sin\beta\cos\beta + P_{uw}\cos 2\beta\Big) = T_E. \end{aligned} \tag{2.43}$$

As done in previous sections, the pitch acceleration term is isolated giving

$$P_{vv}\dot{u}_2 = T_E - T_{DEK1} - T_{DEK2}, \tag{2.44}$$

where the disturbance terms are defined as

$$T_{DEK1} = u_1^2\Big((P_{uu} - P_{ww})\sin\beta\cos\beta + P_{uw}\cos 2\beta\Big), \tag{2.45}$$

$$T_{DEK2} = u_1u_2(P_{uv}\cos\beta - P_{vw}\sin\beta). \tag{2.46}$$

These terms correspond respectively to centrifugal and mixed-velocity cross-coupling effects.

Moving on to the yaw axis, Kane's equation is now evaluated using the generalized speed u_1, which yields the yaw dynamics in the form

$$J_Z(\beta)\dot{u}_1 = T_A - T_{DZ}, \tag{2.47}$$

where the effective yaw-axis inertia is (as before)

$$J_Z(\beta) = Y_{zz} + P_{uu}\sin^2\beta + 2P_{uw}\sin\beta\cos\beta + P_{ww}\cos^2\beta,$$

and T_{DZ} groups gyroscopic, Coriolis, and cross-axis coupling effects, consistent with the NE and Lagrange formulations.

2.4.3 Consistency with NE and Lagrange Formulations

Kane's method yields equations of motion equivalent to those derived using NE and Lagrange methods under the same modelling assumptions. Differences are found only in the grouping of non-linear and cross-coupling terms T_{DEK1} and T_{DEK2}.

2.5 Comparison of Dynamic Formulations

Having described the most common methodologies for modelling the physics of the gimbal, it is now useful to compare the NE, Lagrange-Euler, and Kane formulations, with the objective of clarifying their individual effects on control design and simulation.

Although the three approaches are derived from distinct theoretical foundations, they all describe the same physical system and are formulated under identical modelling assumptions. As a result, when fully expanded, they lead to equivalent non-linear equations of motion. This equivalence may seem like the derivation was a giant waste of time, but aside from the control implications, the consistency of the modelling procedure across different methods guarantees that any observed differences in system behaviour arise from control or implementation choices rather than the underlying physics.

Modelling Assumptions

It was previously stated that all formulations were derived under the same set of assumptions, which is of course a prerequisite for any meaningful comparison. Both the yaw and pitch gimbals are modelled as rigid bodies with constant inertia tensors, and the same reference frames, angular coordinates, and kinematic definitions being used throughout the chapter. Gravitational effects are assumed to be fully compensated, and the base of the system is considered fixed with respect to the inertial frame. Additional simplifications, such as neglecting off-diagonal inertia terms, were deliberately avoided at this stage as retaining these terms gives the model greater flexibility, allowing their influence to be evaluated later if needed as disturbance contributions rather than requiring a reformulation of the equations.

Structural Comparison of the Formulations

The NE formulation presents the system's dynamics directly in terms of angular velocities and angular accelerations while retaining the full inertia tensors and explicitly accounting for all inertial and gyroscopic effects. Cross-axis coupling, transport terms, and velocity-dependent torques appear as distinct components of the torque balance. This explicit structure makes the NE formulation particularly well suited as a reference or benchmark model for simulation and validation. However, the resulting equations are algebraically dense and often call for additional manipulation before being used for control design.

The Lagrange-Euler formulation derives the equations of motion from the kinetic energy of the system using generalized coordinates. In this approach, effective inertia terms naturally emerge from the energy expressions, while coupling and non-linear effects appear as grouped disturbance terms. This results in a more compact and analytically structured representation of the dynamics, which is advantageous for control-oriented modelling and theoretical analysis.

Kane's method reformulates the dynamics in terms of generalized speeds that are chosen to coincide directly with the actuator inputs. This alignment simplifies the interpretation of the equations and leads to a natural separation between inertia-dominated terms and velocity-dependent coupling effects. Although mathematically equivalent to the other formulations, Kane's method emphasizes actuator-level behaviour and is therefore particularly suitable for robustness analysis, decoupling strategies, and controller implementation in systems where precise actuator coordination is critical.

Discussion

While the three formulations differ in presentation and mathematical structure, they describe the same physical phenomena and impose no additional approximations beyond the shared modelling assump-

tions. The differences observed between them are hence a matter of representation rather than physical in nature.

The NE formulation provides the most explicit representation of inertial and gyroscopic effects and is well suited for detailed dynamic analysis and benchmarking. The Lagrange-Euler method provides a compact, energy-based structure that facilitates analytical manipulation and control-oriented applications. Kane's method provides an alternative formulation that highlights actuator dynamics and nonlinear coupling effects in a form that is particularly convenient for control design.

Consequently, the choice between formulations does not affect the physical accuracy of the model but instead influences the clarity, compactness, and usability of the equations for a given application. In the context of this project, these distinctions will directly impact subsequent decisions regarding controller structure, disturbance compensation, and simulation strategy rather than the underlying dynamic behaviour itself.

Chapter 3

Proposed Work

The main component of the thesis, as was previously stated, is the design of the control system which is exactly what the next phase of the project will focus on. Before starting, however it is a good idea to establish the general direction of what's to come.

Firstly, the determination of whether the concept is successfully accomplishing the task at hand, must be made in a formalized manner. The objective of blinding a drone's optical sensor, is in essence the result of the transmission of energy into the lens of said sensor. For that reason, knowing all of the variables that affect the laser irradiance that is delivered beforehand (variables of the laser and atmospheric conditions), all that is missing is the time period during the camera was irradiated. This variable, which we've already denominated as TOT, will serve as the key determinant of a successful simulation and with it, the idea is the building of a set of interception envelopes, with which, depending upon the trajectory undertaken by the UAV and other parameters that are chosen, we may establish when and where the blinding, be it permanent or temporary is possible.

Imperfections and uncertainties in the tracking, laser and control systems will amount to a certain error in the final laser position (compared to the camera's). Taking into account the results obtained in [4], it becomes clear that the resulting error is neither non-existent nor small enough to be disregarded which necessitates some a priori deliberation on what to do in case the magnitude of the error is too large for a direct targetting scenario. Some other factors that haven't yet been formalized include : Losing track and or misidentifying targets, the variation of the cross-sectional area of the laser beam along the flight path and even evasive flying manoeuvres.

A proposed solution to attenuate all of the aforementioned problems is the implementation of a sweeping protocol that screens a wide area with the hope that the accumulated uncertainty from all of the effects from before is still well within the area that was swept.

Below you'll find the current iteration of the project timeline, do note however that this is a merely qualitative representation :

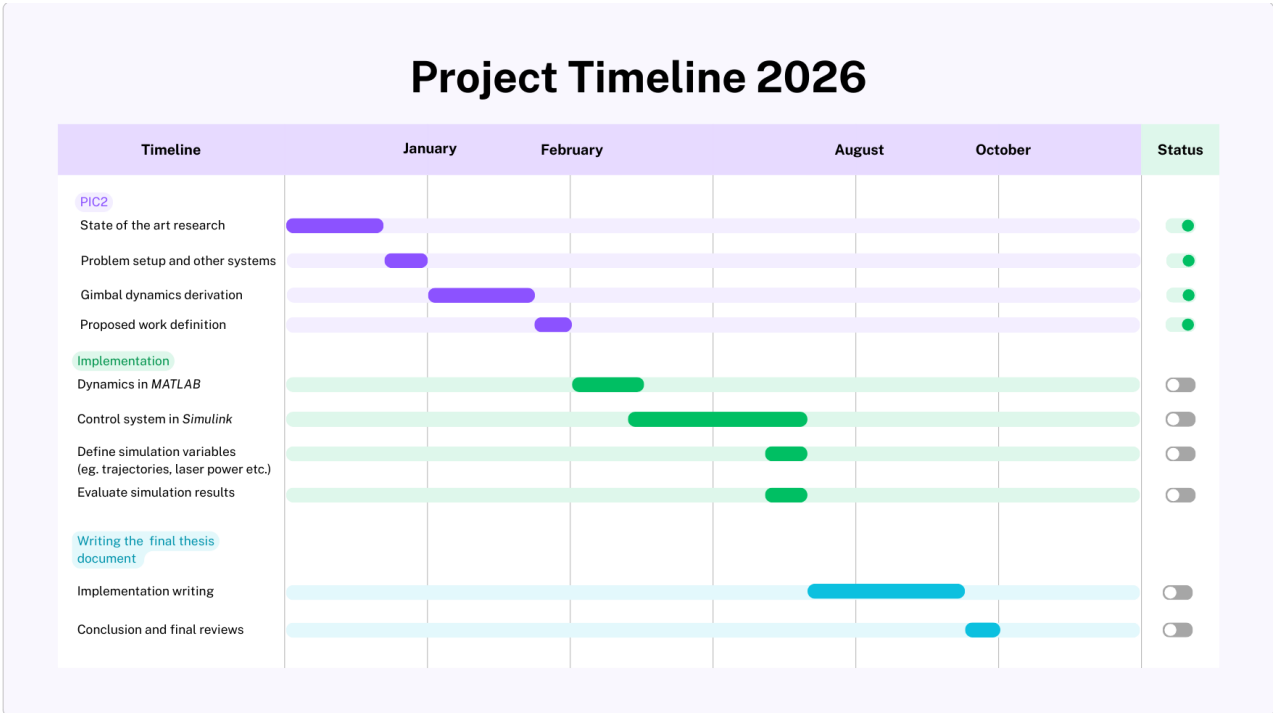

Figure 3.1: Project timeline

Chapter 4

Conclusion

This introductory project's main aim was to evaluate the feasibility of neutralizing unmanned aerial vehicles via the blinding of their optical sensors using a gimbal-mounted, lower-powered laser system. Unlike conventional high-energy laser solutions aimed at structural destruction, the proposed approach trades laser power for increased accuracy, increasing the requirements on tracking and control.

In short, a mathematical framework for a two-degree-of-freedom yaw–pitch gimbal was developed using three alternative dynamic modelling approaches: NE, Lagrange–Euler, and Kane's method. After the detailed derivation of each one, it was demonstrated that all three formulations lead to identical nonlinear, second-order, equations of motion when consistent assumptions are applied. This equivalence validates the modelling process and confirms that the dominant coupling effects namely inertial, gyroscopic, and structure-dependent disturbances are properties of the system rather than particularities of a specific formulation.

The control-oriented decomposition of the dynamics highlights the challenges inherent to the precise control of these type of systems, particularly under simultaneous yaw and pitch motion. Cross-axis coupling, angle-dependent inertia ($J_Z(\beta)$), and velocity-dependent disturbance torques were shown to play a significant role in what torque needed to be provided by the actuator and tracking accuracy, reinforcing the need for realistic dynamic models.

Beyond gimbal dynamics, the project also considered the interception problem within a realistic framework scenario. The limitations of visual tracking, including pixel jitter, range estimation errors, and intermittent target loss, were identified as critical imperfections to the detection and targetting system. Similarly, laser effectiveness was shown to depend not only on the source power but also on atmospheric propagation effects, incidence angle, and irradiation time, all of which contribute directly to the final result.

Taken together, the analysis supports the central premise of this work: that sensor blinding using lower-powered lasers is a feasible counter-UAV strategy, provided that sufficient attention is given to modelling fidelity, control robustness, and system-level integration. The results suggest that improvements in gimbal control design can directly translate into increased engagement envelopes and reduced laser power requirements.

Future work will focus on integrating the derived models into a robust simulation environment, enabling quantitative evaluation of TOT under evasive target trajectories. Alternate solutions for an eventual lack of accuracy include advanced control strategies (sweeping area), adaptive disturbance compensation, and the inclusion of more detailed atmospheric and sensor damage models. Such developments will further clarify the operational viability of precision laser-based C-UAS in complex real-world scenarios.

Bibliography

[1] D.-H. Lee, D.-Q. Tran, Y.-B. Kim, and S. Chakir, "A robust double active control system design for disturbance suppression of a two-axis gimbal system," *Electronics*, vol. 9, no. 10, 2020.

[2] M. Newton, "How are drones changing war? the future of the battlefield," Nov. 2025. Accessed on the 22nd of Nov 2025.

[3] Y. J. Bob, "Israel, us to accelerate production of iron dome, iron beam laser, david's sling missiles," *The Jerusalem Post*, Nov. 2025. Retrieved on the 22 of November 2025.

[4] E. Kuantama, Y. Zhang, F. Rahman, R. Han, J. Dawes, R. Mildren, T. A. Abir, and P. Nguyen, "Laser-based drone vision disruption with a real-time tracking system for privacy preservation," *Expert Systems with Applications*, vol. 255, p. 124626, 2024.

[5] Q. Huang, J. Zhou, X. Chen, Y. Yao, Y. Chen, W. Chen, R. Chen, and Z. Lv, "Modeling and control of a two-axis stabilized gimbal based on kane method," *Sensors*, vol. 24, no. 11, 2024.

[6] B. Ekstrand, "Equations of motion for a two-axes gimbal system," *IEEE Transactions on Aerospace and Electronic Systems*, vol. 37, no. 3, pp. 1083–1091, 2001.

[7] M. H. Ahmad, K. Osman, M. F. M. Zakeri, and S. I. Samsudin, "Mathematical modelling and pid controller design for two dof gimbal system," in *2021 IEEE 17th International Colloquium on Signal Processing Its Applications (CSPA)*, pp. 138–143, 2021.

[8] Y. Bai and D. Wang, "Dynamic modeling of the laser tracking gimbal used in a laser tracking system," *International Journal of Modelling Identification and Control*, vol. 12, pp. 149–159, 01 2011.

[9] E. Poyrazoğlu, "Detailed modeling and control of a 2-dof gimbal system," Master's thesis, Middle East Technical University, 2017.

[10] e. a. Alshaer, "Vision-based uav detection and tracking using deep learning and kalman filter," *Computational Intelligence*, 2025.

[11] A. Koksal, K. G. Ince, and A. Alatan, "Effect of annotation errors on drone detection with yolov3," in *CVPR Workshops*, 2020.

[12] M. authors, "Adg-yolo: A lightweight and efficient framework for real-time uav target detection and ranging," *Drones*, vol. 9, no. 10, 2025.

[13] B. Schwarz, "Laser safety calculations for imaging sensors," *Sensors (Basel)*, vol. 19, no. 17, p. 3799, 2019.

[14] Z. Jian, W. Zhou, H. Chang, Y. Ma, X. Quan, and Z. Wang, "Thermal damage characterization of detector induced by nanosecond pulsed laser irradiation," *Photonics*, vol. 12, no. 8, 2025.

[15] P. Fathi-Hafshejani, A. Soltani-Tehrani, N. Shamsaei, and M. Mahjouri-Samani, “Laser incidence angle influence on energy density variations, surface roughness, and porosity of additively manufactured parts,” *Additive Manufacturing*, vol. 50, p. 102572, 2022.